

Quantum control of entangled photon-pair generation in electron-atom collisions driven by multiphoton-tailored free-electron wave packets

R. Esteban Goetz* and Klaus Bartschat

Department of Physics and Astronomy, Drake University, Des Moines, IA 50311, USA

(Dated: June 24, 2022)

Two-pathway coherent control of photoionization is an example of control of matter waves using light. Here, we analyze the opposite and investigate the control of quantum light using matter waves. We report coherent control of entangled photon-pair emission in electron-atom collisions mediated by transfer of the temporal and atomic coherence carried by the incident electron wave packet. The latter is engineered by resonantly-enhanced multiphoton ionization exploiting interfering ionization pathways. We show that both sources of coherence can be used to control the angular distributions of photons emitted by radiative cascade upon optical decay in the target atom, offering the possibility of coherent control driven by sculpted matter waves via transfer of optical and atomic coherence.

a. Introduction.— Atomic coherence [1] and quantum interferences [2, 3] are the cornerstone of coherent control of quantum phenomena. Control over the constructive and destructive interferences involving the different angular momentum components of the wave packets originating from commensurable interfering photoionization pathways play a pivotal role in the development of coherent control of light over matter waves and are at the heart of two-pathway coherent control of photoionization.

With the advent of bichromatic laser sources [4, 5], free-electron wave-packet interferometry made it possible to exploit such interferences by generating and engineering free-electron wave packets [6, 7]. Typically, coherent control is achieved by manipulating the temporal coherence of the ionizing field, e.g., by modifying the relative phase [8–14] or, alternatively, the time-delay [6, 15] between the different frequency components contributing to the interfering photoionization pathways. The optical and atomic coherence inherited from the interferometric process by the released photoelectron wave packet is imprinted on the photoelectron momentum distribution [6, 7, 16]. Polarization-tailored bichromatic laser fields and high-order intrapulse frequency mixing have also been applied to tailor matter waves [7].

In the above cases, the optical coherence of a light source is devised to exploit atomic coherence and quantum interferences to ultimately control the properties of matter waves. In this Letter, we adopt the opposite approach and investigate the control of quantum light by matter waves, mediated by the temporal and atomic coherences carried by a tailored photoelectron wave packet.

Coherent control of single- and entangled photon-pair states produced by parametric down-conversion using coherent light sources has become a current topic of intense and active research with major impact in photonic quantum information sciences [17–20]. It is thus of paramount importance for the development of new spectroscopy techniques, such as quantum-optical coherence tomogra-

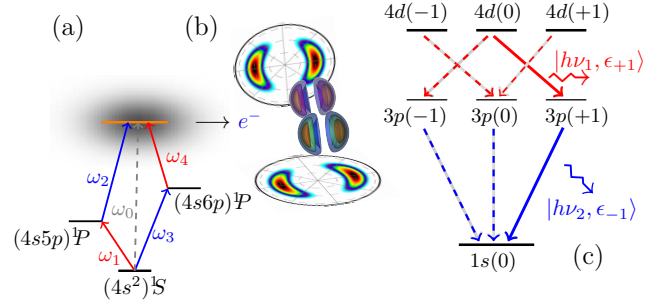


FIG. 1. Matter waves control of correlated photon-pair generation: (a) Ionization of atom A by a classical field probing a manifold of interfering ionization pathways generates a coherent superposition of continuum states that result in the photoelectron wave packet with a momentum distribution depicted in (b). Due to inelastic excitation induced by the electron wave packet upon collision with the target atom B, the optical decay of the latter results in the emission of entangled photon pairs (c).

phy [21, 22], virtual-state spectroscopy [23–26], quantum light-based pump-probe spectroscopy [27–31], and entangled two-photon absorption spectroscopy [32, 33].

For instance, control of fluorescence in single-photon emission has been reported in a four-level system by varying the relative phase between two pump-laser sources with equal frequencies but adjustable relative phase [34]; in a three-level system by adjusting the relative phase between a pump (excitation) and control (driving optical transitions) pulse [35]; by varying the relative phase and amplitude of a trichromatic pump-laser field [36]; and by controlling the Rabi frequency and the phase of a microwave field coupling the two outermost levels in a four-level system [37]. More recently, high degrees of entanglement between parametric-down photons were reported by exploiting the twist phase of a twisted Gaussian pump beam with partial transverse spatial coherence [38]. Control over spontaneous parametric-down photons using chirped pump pulses [39] and the cross section of entangled photon pairs using classical light sources has also been reported [40].

*esteban.goetz@drake.edu

In this Letter, we propose to use matter waves, rather than light, in the form of photoelectron wave packets sculpted by coherent ionizing fields from a manifold of interfering photoionization pathways as the carrier of the coherence required to control two-photon cascade emission after electron-impact excitation. In addition to optical (temporal) coherence, atomic coherence inherited by the tailored photoelectron wave packet from a pump-probe spectroscopic preparation may also be exploited as a source of control. The purpose of this work is to elucidate the extent to which both sources of coherence can be transmitted to the tailored electron wave packet to ultimately manipulate entangled photon-pair generation in electron-atom collisions.

b. Theoretical model.— The atom-photon field interaction is treated at the level of the Weisskopf-Wigner theory for spontaneous emission [41]. De-excitation of atom B occurring during and after collision with the incident electron wave packet yields the photon field in an excited multimode state. The basis,

$$|n_{\mathbf{k}_1, \sigma_1}, n_{\mathbf{k}_2, \sigma_2}, \dots\rangle = \prod_{\mathbf{k}_j, \sigma_j} |n_{\mathbf{k}_j, \sigma_j}\rangle, \quad (1)$$

represents $n_{\mathbf{k}_j, \sigma_j}$ photons in mode (\mathbf{k}_j, σ_j) : momentum $\hbar\mathbf{k}_j$ and polarization $\hat{\mathbf{e}}_{\sigma_j}$ subject to the transversality conditions $\hat{\mathbf{e}}_{\sigma_j} \cdot \mathbf{k}_j = 0$. The target atom and photon field are coupled via the terms $\hat{\mathbf{A}}_s(\hat{\mathbf{r}}) \cdot \hat{\mathbf{p}}$ and $\hat{\mathbf{A}}_s(\hat{\mathbf{r}}) \cdot \hat{\mathbf{A}}_s(\hat{\mathbf{r}})$, with

$$\hat{\mathbf{A}}_s(\hat{\mathbf{r}}) = \sum_{\mathbf{k}_j, \sigma_j} A_0(k_j) \left[\hat{\mathbf{a}}_{\mathbf{k}_j, \sigma_j} e^{i\mathbf{k}_j \cdot \hat{\mathbf{r}}} \hat{\mathbf{e}}_{\sigma_j} + \hat{\mathbf{a}}_{\mathbf{k}_j, \sigma_j}^\dagger e^{-i\mathbf{k}_j \cdot \hat{\mathbf{r}}} \hat{\mathbf{e}}_{\sigma_j} \right] \quad (2)$$

as the vector potential operator coupling the eigenstates of B with the photon field. $\hat{\mathbf{a}}_{\mathbf{k}_j, \sigma_j}^\dagger$ ($\hat{\mathbf{a}}_{\mathbf{k}_j, \sigma_j}$) creates (annihilates) one photon in mode (\mathbf{k}_j, σ_j) . The Hamiltonian,

$$\hat{\mathbf{H}}_{AB}(t) = \left[\hat{\mathbf{H}}_A - e\hat{\mathbf{r}} \cdot \hat{\mathbf{E}}(\hat{\mathbf{r}}, t) \right] \otimes \mathbb{1} + \hat{\mathbf{V}}_I \quad (3a)$$

$$+ \mathbb{1} \otimes \left[\sum_{\mathbf{k}_j, \sigma_j} \hbar\omega(\mathbf{k}_j) + \frac{1}{2m} \left(\hat{\mathbf{p}} - \frac{e}{c} \hat{\mathbf{A}}_s(\hat{\mathbf{r}}, t) \right)^2 \right],$$

dictates the ionization dynamics of atom A , scattering of the resulting photoelectron wave packet by atom B , excitation of the latter due to collision, and photoemission upon de-excitation of atom B . The interaction,

$$\hat{\mathbf{V}}_I = \frac{e^2}{\hat{\mathbf{r}} - \hat{\mathbf{r}}'} + V_{ne}^B(\hat{\mathbf{r}} - \mathbf{r}_{0,B}) \otimes \mathbb{1} + \mathbb{1} \otimes V_{ne}^B(\hat{\mathbf{r}} - \mathbf{r}_{0,B}), \quad (3b)$$

mediates the scattering as well as elastic and inelastic excitations of atom B with no change in the distribution of the photon modes. Ionization of atom A is controlled by the classical field $\mathbf{E}(\mathbf{r}, t) = \mathbf{E}(t) f_{\Omega_A}(\mathbf{r})$, with $f_{\Omega_A}(\mathbf{r})$ a Heaviside function. The latter ensures a constant spatial distribution in the vicinity of atom A and leaves the target atom B unaffected. $V_{ne}^B(\hat{\mathbf{r}} - \mathbf{r}_{0,B})$ is the potential energy due to the effective charge distribution acting

on the single active electron of atom B in the absence of atom A , with $\mathbf{r}_{0,B}$ the (fixed) origin of the coordinates of B with respect to A . Equation (B1) is written in the basis $|\psi_{\gamma_a}^A\rangle \otimes |\psi_{\gamma_b}^B\rangle \otimes |n_{\mathbf{k}_1, \sigma_1}, n_{\mathbf{k}_2, \sigma_2}, \dots\rangle$, with $|\Phi_{\gamma_a}^A\rangle$ and $|\Phi_{\gamma_b}^B\rangle$ as the eigenvectors of the isolated Hamiltonians $\hat{\mathbf{H}}_A$ and $\hat{\mathbf{H}}_B$. They satisfy $\hat{\mathbf{H}}_A|\Phi_{\gamma_a}^A\rangle = \epsilon_{\gamma_a}^A|\Phi_{\gamma_a}^A\rangle$ and $\hat{\mathbf{H}}_B|\Phi_{\gamma_b}^B\rangle = \epsilon_{\gamma_b}^B|\Phi_{\gamma_b}^B\rangle$, respectively.

We solve the time-dependent Schrödinger equation

$$i \frac{\partial}{\partial t} |\Psi_S(t)\rangle = \hat{\mathbf{H}}_{AB}(t) |\Psi_S(t)\rangle, \quad (4a)$$

and write $|\Psi_S(t)\rangle$ as a coherent superposition in the antisymmetrized tensor product space spanned by the eigenvectors of the isolated Hamiltonians and Eq. (1), i.e.,

$$|\Psi_S(t)\rangle = \sum_{\gamma_a^A, \gamma_b^B} \sum_{n_{\mathbf{k}_1, \sigma_1}} \sum_{n_{\mathbf{k}_2, \sigma_2}} \dots |\Phi_{\gamma_a^A, \gamma_b^B}\rangle \otimes \prod_{\mathbf{k}_j, \sigma_j} |n_{\mathbf{k}_j, \sigma_j}\rangle$$

$$\times \exp \left[-i \left(\epsilon_{\gamma_a}^A + \epsilon_{\gamma_b}^B + \sum_{\mathbf{k}_i, \sigma_i} \omega(\mathbf{k}_i) n_{\mathbf{k}_i, \sigma_i} \right) t \right]$$

$$\times S_{\gamma_a^A, \gamma_b^B}(n_{\mathbf{k}_1, \sigma_1}, n_{\mathbf{k}_2, \sigma_2}, n_{\mathbf{k}_3, \sigma_3} \dots; t). \quad (4b)$$

The vector $|\Phi_{\gamma_a^A, \gamma_b^B}\rangle \equiv |\Phi_{\gamma_a^A}^A\rangle \otimes |\Phi_{\gamma_b^B}^B\rangle - |\Phi_{\gamma_b^B}^B\rangle \otimes |\Phi_{\gamma_a^A}^A\rangle$ represents one electron in a spin-orbital state $\langle \mathbf{r}_1; m_{s_1} | \Phi_{\gamma_a^A}^A \rangle$ of A and the other one in $\langle \mathbf{r}_2; m_{s_2} | \Phi_{\gamma_b^B}^B \rangle$ of B with $m_{s_{1,2}}$ the spin-magnetic quantum numbers for electrons 1 and 2. Note that $\langle \mathbf{r}_1, m_{s_1}; \mathbf{r}_2, m_{s_2} | \Phi_{\gamma_a^A, \gamma_b^B} \rangle = -\langle \mathbf{r}_2, m_{s_2}; \mathbf{r}_1, m_{s_1} | \Phi_{\gamma_a^A, \gamma_b^B} \rangle$. Summation over γ_a^A includes all bound and continuum states, and $\omega(\mathbf{k}_j) = |\mathbf{k}_j|c$. Matrix elements to describe the ionization process were obtained with the B-spline R-matrix codes [42].

Due to the many-body character of the stimulated photon field, a full time-dependent treatment of the dynamics, while keeping track of every possible photon mode emitted and absorbed during the aforementioned processes, is a formidable and computationally prohibitive task. To scrutinize the control mechanisms for radiative photon cascade emission triggered by the collision while keeping the calculations tractable, we resort to obtain the coefficients in Eq. (4b) from a time-dependent perturbative series expansion up to order k . Details are provided in the Appendix.

c. Inelastic excitation-decay control mechanism.—

We start by considering resonantly-enhanced two-pathway coherent ionization of Ca as schematically depicted in Fig. 1(a). Resonant excitation of the $(4s5p)^1P$ and $(4s6p)^1P$ states is mediated by the frequency components $\omega_1 = 4.554$ eV and $\omega_3 = 5.167$ eV of a classical field, both left-circularly polarized. Their relative phase is used as a control parameter. Ionization is ensured by the linearly polarized frequency components $\omega_2 = 17.324$ eV and $\omega_4 = 16.701$ eV with a flat spectral phase. The frequency components have a duration of 20 fs (FWHM) and are not time-delayed. Each ionization pathway generates

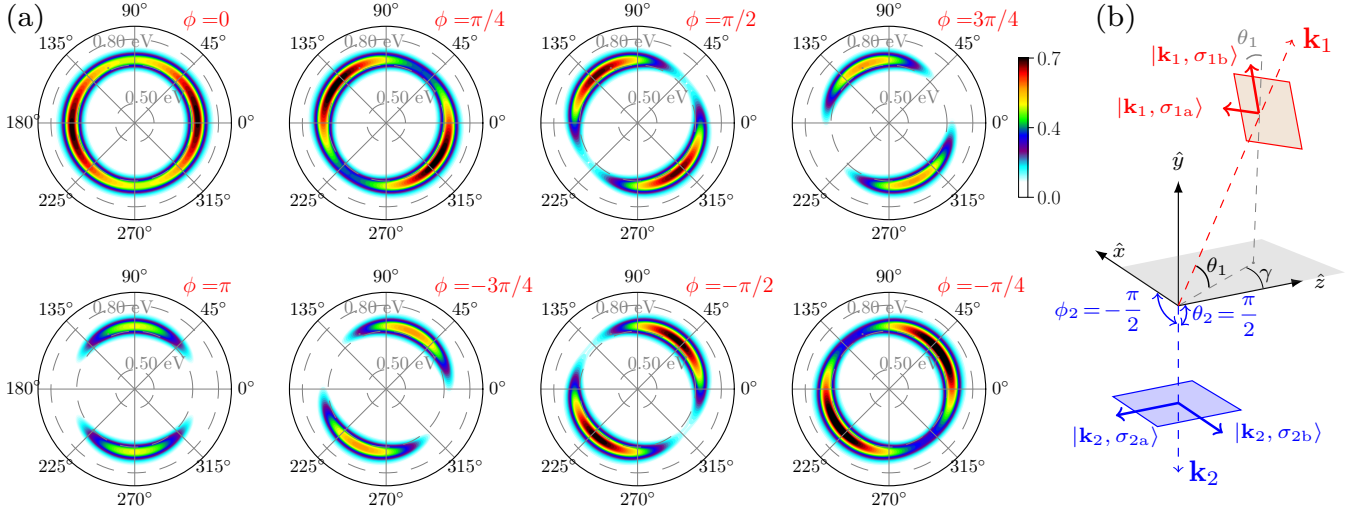


FIG. 2. **Inelastic excitation-decay control mechanism:** (a) Angular distribution of correlated photon-pair emission as a function of the relative phase, ϕ , between the laser frequencies ω_1 and ω_3 shown in Fig. 1(a). The incident photoelectron wave packet results from a coherent superposition of even-parity two-photon ionization pathways. Note that the angular probability of photodetection follows the relative phase. (b) Correlated photon-pair detection scheme discussed in the text ($\gamma = 0$).

a coherent superposition of continuum eigenstates of A peaked at the same photoelectron energy of 15.755 eV, as depicted in Fig. 1(b). The angular-momentum components defining the wave packets that arise from each of these ionization channels are coherently combined, carrying the temporal coherence of the classical field.

The target atom B , initially in its ground state, is taken as the hydrogen atom. After excitation by the electron wave packet, optical decay may occur via different de-excitation pathways allowed by the selection rules, as epitomized in Fig. 1(c). The angular distribution of the emitted photons is obtained using the multipole expansion in Eq. (2),

$$e^{\pm i \mathbf{k}_j \cdot \mathbf{r}} = 4\pi \sum_{\lambda, \mu} (\pm i)^\lambda j_\lambda(k_j r) Y_\mu^\lambda(\theta_r, \phi_r) Y_\mu^{\lambda*}(\theta_{k_j}, \phi_{k_j}), \quad (5)$$

with the spherical harmonics $Y_\mu^\lambda(\theta_{k_j}, \phi_{k_j})$ for the angles of photoemission defining the mode (\mathbf{k}_j, σ_j) . For the photon energies considered in this work, the wavelength is several orders of magnitude larger than the extension of the highest bound state considered in our calculations. We therefore approximate the Bessel functions as $j_\lambda(k_j r) \approx (k_j r)^\lambda / (2\lambda + 1)!!$ for $k_j r \ll 1$, which allows us to obtain the transition matrix elements as a power series in r^λ . The polarization components of the emitted photons are obtained according to $\hat{\mathbf{e}}_{\sigma_{ja}} = \mathbf{k}_j \times \hat{\mathbf{e}}_0 / |\mathbf{k}_j \times \hat{\mathbf{e}}_0|$ and $\hat{\mathbf{e}}_{\sigma_{jb}} = \mathbf{k}_j \times \hat{\mathbf{e}}_{\sigma_{ja}} / |\mathbf{k}_j \times \hat{\mathbf{e}}_{\sigma_{ja}}|$, where

$$\mathbf{k}_j = (4\pi/3)^{1/2} |\mathbf{k}_j| \sum_{q=0, \pm 1} Y_q^1(\theta_{k_j}, \phi_{k_j}) \hat{\mathbf{e}}_q^*, \quad (6)$$

with $\hat{\mathbf{e}}_q$ the covariant spherical unit vectors. Both polarization vectors are functions of the angles $(\theta_{k_j}, \phi_{k_j})$. The number of de-excitation pathways describing the radiative cascade emission is determined by the maximum

order in the perturbation expansion. The results presented here were obtained by iterating the expansion coefficients up to $k=6$, corresponding to the lowest order to describe the process of radiative two-photon cascade emission while considering feedback effects of the emitted photons on the scattered electron wave packet.

The coincidence photodetection scheme is shown in Fig. 2(b): a first photodetector, fixed at $\theta_{k_2} = \pi/2$ and $\phi_{k_2} = -\pi/2$, measures the polarization component along the z -axis in Fig. 2(b) of a photon with energy $h\nu_2 = 12.078$ eV, corresponding to the radiative transition $3p(m=\pm 1, 0) \rightarrow 1s(m=0)$ in Fig. 1(c). The state of such photon is hereafter referred to as mode (2).

A second detector, fixed at $\phi_{k_1} = \pi/2$ but free to move along the polar coordinate θ_{k_1} , scans, along θ_{k_1} , the direction of emission of the entangled peer defined by the state $|\mathbf{k}_1, \sigma_{1b}\rangle$ in Fig. 2(b): a photon of energy $h\nu_1 = 0.661$ eV, corresponding to the radiative transition $4d(\{m\}) \rightarrow 3p(\pm 1, 0)$ with polarization component along $\hat{\mathbf{e}}_{\sigma_{1b}}$.

Figure 2(a) shows the angular probability distribution of measuring the correlated photon in coincidence with its entangled peer in mode (2) as a function of the relative phase between the frequencies ω_1 and ω_3 of Fig. 1(a). The direction of emission exhibits a noticeable dependence on the temporal coherence conveyed by the incident photoelectron wave packet: the probability of entangled photon-pair detection is strongly affected by the relative phase between the interfering ionization pathways from which the photoelectron originates, controlled by the relative phase between the frequency components of the classical field probing the contributing photoionization pathways.

The angle-resolved occurrence of coincident photo-

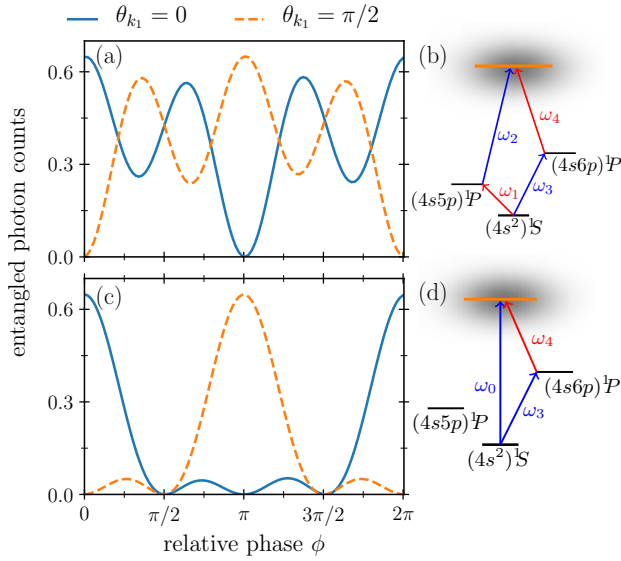


FIG. 3. (a) Photodetection probability at angles $\theta_{k_1} = 0$ (solid blue line) and $\theta_{k_1} = \pi/2$ (dashed orange line) as a function of the relative phase between the laser frequencies ω_1 and ω_3 shown in (b) when a photon in mode (2) is simultaneously detected. The incident electron wave packet originates from the ionization scheme shown in (b). (c) Same as (a) but as a function of the relative phase between the laser frequencies ω_0 and ω_3 shown in (d).

detection is also sensitive to the parity of the photoionization pathways probed to engineer the incident photoelectron wave packet. This is shown in Fig. 3, comparing, at the fixed emission angles $\theta_{k_1} = 0$ and $\theta_{k_1} = \pi/2$, the probability of coincident photodetection already discussed in Fig. 2, this time using different photoionization schemes to engineer the incident electron wave packet: same- and opposite-parity photoionization pathways.

Figure 3(a) displays the probability of coincident photodetection obtained when the incident photoelectron wave packet is engineered according to the resonantly-enhanced two-photon ionization scheme promoting even-parity pathways depicted in Fig. 3(b). As shown in Fig. 3(a), the probability for simultaneous photon-pair detection at a given direction θ_{k_1} can be entirely suppressed or enhanced depending on the relative phase between the contributing photoionization pathways.

Likewise, as shown in Fig. 3(c), opposite-parity photoionization pathways, as depicted in Fig. 3(d), can also be exploited to engineer the photoelectron wave packet to ultimately suppress or enhance the probability of correlated photon-pair detection. In this case, control is achieved by manipulating the relative phase between the one- and two-photon ionization pathways through the relative phase between the frequencies ω_0 and ω_3 .

As defined, the relative phase corresponding to $\phi = 0$ maximize (minimize) the probability of detection in the direction $\theta_{k_1} = 0$ ($\theta_{k_1} = \pi/2$) for both photoionization schemes depicted in Figs. 3(b) and (d) when a photon in mode (2) is simultaneously detected. Conversely,

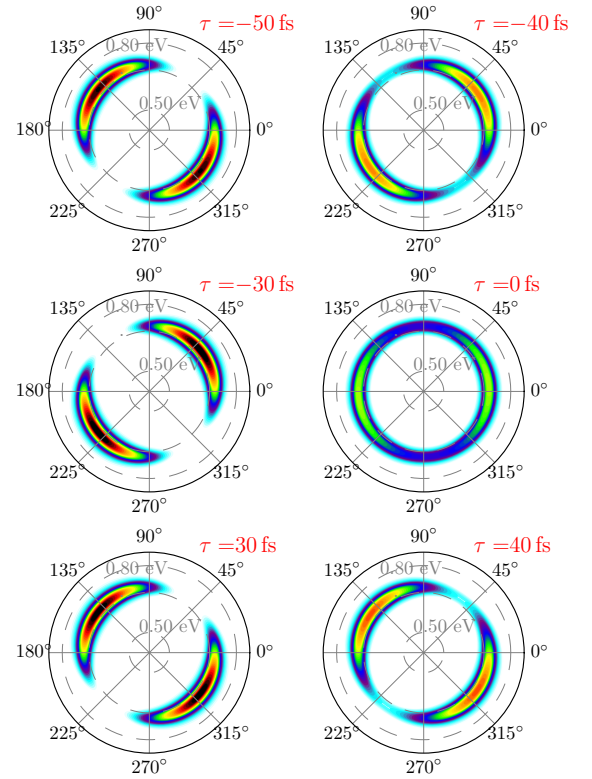


FIG. 4. Time-resolved probability for coincident photodetection as a function of the time delay between the pump and probe pulses discussed in the text. Colormap as in Fig. 2.

for $\phi = \pi$, the probability of detection in the direction $\theta_{k_1} = 0$ ($\theta_{k_1} = \pi/2$) is minimized (maximized) for both schemes. In contrast, the relative phases corresponding to $\phi = \pi/2$ and $\phi = 3\pi/2$ results in the suppression of entangled photon-pair coincident detection at angles $\theta_{k_1} = 0$ and $\theta_{k_1} = \pi/2$ for the case of odd-even parity photoionization pathway (cf. Fig. 3(c)), whereas its even-parity counterpart results in an equal probability of coincidence photodetection, cf. Fig. 3(a).

Finally, we consider the case of coherent control of two-photon cascade emission by transfer of atomic coherence. For this scenario, we choose two pump-laser frequencies, ω_1 and ω_3 , to resonantly excite the states $(4s5p)^1P$ and $(4s6p)^1P$ in atom *A*, creating a superposition of states evolving according to the free-field Hamiltonian. After a delay τ , a probe field with frequencies ω_2 and ω_4 is introduced, ionizing the electron in the coherent superposition. The resulting photoelectron wave packet then carries the atomic coherence defined by the phase accumulated between the pump and probe pulses. Figure 4 shows the time-resolved probability of correlated photon-pair detection as a function of the delay between the pump and probe pulses. The probability for coincident photodetection is sensitive to the atomic coherence carried by the photoelectron wave packet. For a fixed direction θ_{k_1} , the photon yield can be controlled significantly. Compare, for example, the yields at $\theta_{k_1} = 45^\circ$ for the

delays $\tau = -50$ fs and $\tau = -40$ fs.

When a photon in mode (2) is detected, several de-excitation pathways may contribute to the detected polarization: the first detector cannot determine the de-excitation pathway taken by the photon of energy $h\nu_2$ in the second step of the cascade, cf. Fig.1(c), blue arrows. Consequently, it is not possible either to determine the pathway taken by the photon of energy $h\nu_1$ in the first step of the cascade, cf. Fig.1(c), red arrows. The angular distribution of the photon of energy $h\nu_1$ therefore contains a superposition of such contributions. These depend on the population and phase of the $4d(m)$ states and can be adjusted by controlling the ionization process generating the photoelectron wave packet.

d. Conclusions.— Motivated by the recent developments in free-electron wave packet interferometry and engineering, and the increasingly active research in coherent control of entangled photon pair generation, we investigated the generation and control of correlated photon pairs triggered by electron-atom collisions. In contrast to standard approaches, we demonstrated the possibility of controlling quantum light employing engineered matter waves. Using calcium and hydrogen as prototypes to control two-photon cascade emission triggered by electron-atom collisions, we demonstrated that quantum interferences and atomic coherences can be manipulated to coherently control single-photon and correlated photon-pair generation based on the transfer of optical and atomic coherences. Our results can be extended to more complex cases, such as chiral molecules, with the potential to reveal new insights into the interaction of quantum light with chiral matter waves. We also foresee extending our approach to the case of electron-ion collisions to investigate the control of correlated photon-pair emission mediated by electron-trapping correlated decay.

This work was supported by the National Science Foundation under grant No. PHY-1803844.

Appendix A: Hamiltonian system

1. Isolated Hamiltonians

In order to keep the calculations tractable, we consider two initially isolated, non-interacting atomic systems, labelled A and B , with Hamiltonians

$$\hat{H}_A = \sum_{i=1}^{N_A} \left(\frac{\hat{\mathbf{p}}_i^2}{2m} + V_{ne}^A(\hat{\mathbf{r}}_i - \hat{\mathbf{R}}_A) + \sum_{i'>i}^{N_A} V_{ee}(\hat{\mathbf{r}}_i - \hat{\mathbf{r}}_{i'}) \right) \quad (\text{A1a})$$

corresponding to that of the atom from which the photoelectron wave packet is released, and

$$\hat{H}_B = \sum_{j=1}^{N_B} \left(\frac{\hat{\mathbf{p}}_j^2}{2m} + V_{ne}^B(\hat{\mathbf{r}}_j - \hat{\mathbf{R}}_B) + \sum_{j'>j}^{N_B} V_{ee}(\hat{\mathbf{r}}_j - \hat{\mathbf{r}}_{j'}) \right), \quad (\text{A1b})$$

for the target atom. They fulfill $\hat{H}_A|\Phi_{\gamma_a^A}^A\rangle = \epsilon_{\gamma_a^A}^A|\Phi_{\gamma_a^A}^A\rangle$ and $\hat{H}_B|\Phi_{\gamma_b^B}^B\rangle = \epsilon_{\gamma_b^B}^B|\Phi_{\gamma_b^B}^B\rangle$ with eigenvalues $\epsilon_{\gamma_a^A}^A$ ($\epsilon_{\gamma_b^B}^B$), where

γ_a^A (γ_b^B) collectively denotes a set of quantum numbers that uniquely define the states $|\Phi_{\gamma_a^A}^A\rangle$ and $|\Phi_{\gamma_b^B}^B\rangle$.

The summations are over the N_A and N_B electrons of atom A and B , respectively. $\hat{\mathbf{V}}_{ee}$ is the electron-electron potential energy operator and $\hat{\mathbf{R}}_A$ ($\hat{\mathbf{R}}_B$) the position operator acting on the nuclear wavefunction of A (B).

Recoil is not considered. The origins of the coordinate systems are $\mathbf{R}_{0,A}$ ($\mathbf{R}_{0,B}$), defined by the (fixed) position of the point-like nuclear charge distribution assumed to be of the form $Z_A \delta(\mathbf{R}_A - \mathbf{R}_{A,0})$ ($Z_B \delta(\mathbf{R}_B - \mathbf{R}_{B,0})$) with Z_A (Z_B) as the effective nuclear charge. The distance $|\mathbf{R}_{0,A} - \mathbf{R}_{0,B}|$ is taken such that $\langle \Phi_{\gamma_a^A}^A | \Phi_{\gamma_b^B}^B \rangle = 0$ for all bound states. We denote by \mathcal{H}_A and \mathcal{H}_B the Hilbert spaces spanned by the eigenvectors of the Hamiltonians defined in Eqs. (A1a) and (A1b), respectively.

2. Optical preparation and laser-induced ionization

The optical preparation and ionization of atom A is mediated by a classical field $\mathbf{E}(\mathbf{r}, t)$ parameterized as

$$\mathbf{E}(\mathbf{r}, t) = \sum_{\mu_0} \sum_{n=1}^N h_{\mu_0}^{(n)}(t - \tau_n) \text{Re} \left\{ e^{-i\Phi_n(t - \tau_n)} \mathbf{e}_{\mu_0} \right\} f_{\Omega_A}(r), \quad (\text{A2})$$

with N frequency components ω_n and instantaneous frequencies $\Phi_n(t) = \omega_n t + \tilde{\varphi}_n$, where $\tilde{\varphi}_n = -\omega_n \tau_n + \phi_n$ is the spectral phase, ϕ_n the carrier envelope phase (CEP), and τ_n the time delay with respect to $t = 0$. $h^{(n)}(t - \tau_n)$ is a Gaussian function with adjustable amplitude centered around τ_n . Left-circular ($\mathbf{e}_{-1} = (\mathbf{e}_x - i\mathbf{e}_y)/\sqrt{2}$), right-circular ($\mathbf{e}_{+1} = -(\mathbf{e}_x + i\mathbf{e}_y)/\sqrt{2}$), and linear ($\mathbf{e}_0 = \mathbf{e}_z$) polarization states are described by \mathbf{e}_{μ_0} . The photoelectron wave packet resulting from ionization of A is controlled by means of these field parameters.

To avoid treating the collision dynamics in the presence of a dressing background field, the Heaviside function $f_{\Omega_A}(r)$ ensures a constant amplitude for the spatial distribution of \mathbf{E} within the region defined by the extension of the outermost excited state of atom A . Being zero elsewhere, the target atom B is not affected by the field.

Appendix B: Equations of motion

1. Perturbation expansion

To illustrate our idea of coherent control at a reduced computational cost, we treat the ionization of atom A (here calcium) and the collision of the resulting photoelectron wave packet with the target atom B (here atomic hydrogen) as an effective two-electron problem. The Hamiltonian,

$$\hat{H}_{AB}(t) = [\hat{H}_A - e \hat{\mathbf{r}} \cdot \hat{\mathbf{E}}(\hat{\mathbf{r}}, t)] \otimes \mathbb{1} + \hat{\mathbf{V}}_I \quad (\text{B1})$$

$$+ \mathbb{1} \otimes \left[\sum_{\mathbf{k}_j, \sigma_j} \hbar \omega(\mathbf{k}_j) + \frac{1}{2m} \left(\hat{\mathbf{p}} - \frac{e}{c} \hat{\mathbf{A}}_s(\hat{\mathbf{r}}, t) \right)^2 \right],$$

with $\hat{\mathbf{A}}_s$ the vector potential describing the photon field, dictates the ionization dynamics of atom A , scattering of the resulting photoelectron wave packet by atom B , collision-induced excitation of the latter, and photoemission upon de-excitation of atom B . The interaction $\hat{\mathbf{V}}_I$, mediating elastic scattering from as well as excitation of atom B without change in the distribution of photon modes is defined in Eq. (3b).

We search for a solution, $|\Psi_S(t)\rangle$, satisfying

$$i\frac{\partial}{\partial t}|\Psi_S(t)\rangle = \hat{\mathbf{H}}_{AB}(t)|\Psi_S(t)\rangle. \quad (\text{B2a})$$

To keep the calculations tractable, we employ a time-dependent perturbative series expansion for

$$|\Psi_S(t)\rangle \approx |\Psi_S^{(0)}(t)\rangle + \sum_{k=1}^{k_{\max}} |\Psi_S^{(k)}(t)\rangle. \quad (\text{B2b})$$

The zeroth-order term, $|\Psi_S^{(0)}(t)\rangle$, describes the isolated atoms A and B in their respective ground states $|\Phi_{\gamma_a^0}^A\rangle$ and $|\Phi_{\gamma_b^0}^B\rangle$ and the photon field in the vacuum state

$$|\Psi_S^{(0)}(t)\rangle = e^{-i(\epsilon_{\gamma_a^0}^A + \epsilon_{\gamma_b^0}^B + 1/2)t} \times \left[|\Phi_{\gamma_a^0}^A\rangle \otimes |\Phi_{\gamma_b^0}^B\rangle - |\Phi_{\gamma_b^0}^B\rangle \otimes |\Phi_{\gamma_a^0}^A\rangle \right] \otimes |0\rangle. \quad (\text{B2c})$$

At intermediate times, $|\Psi_S(t)\rangle$ is written as a coherent superposition in the antisymmetrized tensor product space spanned by the eigenvectors of the isolated Hamiltonians and a coherent multimode photon field,

$$|\Psi_S^{(k+1)}(t)\rangle = \sum_{\gamma_a^A, \gamma_b^B} \sum_{n_{\mathbf{k}_1, \sigma_1}} \sum_{n_{\mathbf{k}_2, \sigma_2}} \dots |\Phi_{\gamma_a^A, \gamma_b^B}\rangle \otimes \prod_{\mathbf{k}_j, \sigma_j} |n_{\mathbf{k}_j, \sigma_j}\rangle \times \exp \left[-i \left(\epsilon_{\gamma_a^A}^A + \epsilon_{\gamma_b^B}^B + \sum_{\mathbf{k}_i, \sigma_i} \omega(\mathbf{k}_i) n_{\mathbf{k}_i, \sigma_i} \right) t \right] \times S_{\gamma_a^A, \gamma_b^B}^{(k+1)}(n_{\mathbf{k}_1, \sigma_1}, n_{\mathbf{k}_2, \sigma_2}, n_{\mathbf{k}_3, \sigma_3} \dots; t), \quad (\text{B2d})$$

where $|\Phi_{\gamma_a^A, \gamma_b^B}\rangle \equiv |\Phi_{\gamma_a^A}^A\rangle \otimes |\Phi_{\gamma_b^B}^B\rangle - |\Phi_{\gamma_b^B}^B\rangle \otimes |\Phi_{\gamma_a^A}^A\rangle$.

2. Observables

The expansion coefficients in Eq. (B2d) are used to evaluate the angle-resolved correlated probability of photon-pair emission according to

$$\frac{d^2 \sigma_{n_f}}{d(h\nu_1) d\Omega_{\mathbf{k}_1}} = \int d^3 p_a^A \left| \sum_{k=0}^{k_{\max}} S_{\mathbf{p}_a^A, \gamma_b^B}^{(k)}(\mathbf{n}_f; t \rightarrow \infty) \right|^2, \quad (\text{B3})$$

where the incoherent summation (integration) is performed over the momenta of the scattered photoelectron. Ionization of atom B by electron impact is not considered. Thus, at $t \rightarrow \infty$, atom B returns to its ground state defined by the quantum numbers γ_b^B . At intermediate

times, the photon field may be excited following complex emission and absorption dynamics. The photon-field configuration \mathbf{n}_f in Eq. (B3) specifies the distribution of the photon modes of interest at $t \rightarrow \infty$.

The photon-field configuration corresponding to the radiative two-photon cascade emission depicted in Figs. 1(c) and 2(b), corresponds to the distribution of modes defined by $\mathbf{n}_f = [0, 0, \dots, 1_{m_1}, \dots, 0, \dots, 1_{m_2}, 0, \dots]^T$, where m_2 denotes the mode of photon (2). It is defined by the photon energy $h\nu_2 = 12.078 \text{ eV}$, polarization component along σ_{2a} in Fig. (2b), and direction of photodetection defined by the (fixed) angles $\theta_{k_2} = \pi/2$ and $\phi_{k_2} = -\pi/2$ in Fig. (2b). For additional details, see Sec. C1b below. On the other hand, m_1 denotes the photon mode defined by $h\nu_1 = 0.661 \text{ eV}$, polarization component along $\sigma_{1b}(\theta_{k_1})$ in Fig. (2b), as the photon in mode (1) is detected as a function of the angle θ_{k_1} , cf. Sect. C1b.

3. Propagation of the time-dependent coefficients

To alleviate the notation, we introduce the occupation number representation

$$\mathbf{n} = \begin{bmatrix} n_1 \\ n_2 \\ n_3 \\ \vdots \\ n_p \\ \vdots \end{bmatrix}, \quad \mathbf{n} \pm \mathbf{1}_p = \begin{bmatrix} n_1 \\ n_2 \\ n_3 \\ \vdots \\ n_p \pm 1 \\ \vdots \end{bmatrix}, \quad \mathbf{n} \pm \mathbf{2}_p = \begin{bmatrix} n_1 \\ n_2 \\ n_3 \\ \vdots \\ n_p \pm 2 \\ \vdots \end{bmatrix} \quad (\text{B4})$$

and $|\mathbf{n}\rangle = |n_1, n_2, \dots, n_p, \dots\rangle$. The indices run over all photon modes, hereafter referred to as Ω_γ .

The time-dependent expansion coefficients in Eq. (B2d) are obtained by projecting Eq. (B2a) onto $|\Phi_{\gamma_a^A}^A \Phi_{\gamma_b^B}^B; \mathbf{n}'\rangle$ and iteratively solving the recursive equation

$$S_{\gamma_a^A, \gamma_b^B}^{(k+1)}(\mathbf{n}'; t) = \int_{-\infty}^t \langle \Phi_{\gamma_a^A}^A \Phi_{\gamma_b^B}^B; \mathbf{n}' | \tilde{\Psi}^{(k)}(t') \rangle dt' + \sum_{\gamma_a^A, \gamma_b^B} \left[S_{\gamma_a^A, \gamma_b^B}^{(k)}(\mathbf{n}'; t) e^{(\epsilon_{\gamma_a^A}^A + \epsilon_{\gamma_b^B}^B - \epsilon_{\gamma_a^A}^A - \epsilon_{\gamma_b^B}^B)t} \right]_{t_0}^t \times \langle \Phi_{\gamma_a^A}^A | \Phi_{\gamma_b^B}^B \rangle \langle \Phi_{\gamma_b^B}^B | \Phi_{\gamma_a^A}^A \rangle. \quad (\text{B5a})$$

with $t_0 \rightarrow -\infty$. The integrand in Eq. (B5a) reads

$$\langle \Phi_{\gamma_a^A}^A \Phi_{\gamma_b^B}^B; \mathbf{n}' | \tilde{\Psi}^{(k)}(t') \rangle = \prod_{s \in \Omega_\gamma} e^{i(\epsilon_{\gamma_a^A}^A + \epsilon_{\gamma_b^B}^B + \hbar n_s' \omega_s) t'} \times \langle \Phi_{\gamma_a^A}^A \Phi_{\gamma_b^B}^B; \mathbf{n}' | \hat{\mathbf{H}}_I(t') | \Psi_S^{(k)}(t') \rangle. \quad (\text{B5b})$$

Here we have defined, upon expansion of the quadratic term in Eq. (B1),

$$\hat{\mathbf{H}}_I(t) = \left[-e \hat{\mathbf{r}} \cdot \hat{\mathbf{E}}(\hat{\mathbf{r}}, t) + V_{ne}^B(\hat{\mathbf{r}} - \mathbf{r}_{0,B}) \right] \otimes \mathbb{1} + \hat{\mathbf{V}}_{1,2}(\hat{\mathbf{r}}, \hat{\mathbf{r}}') + \mathbb{1} \otimes \left[-\frac{e}{mc} \hat{\mathbf{A}}_s(\hat{\mathbf{r}}) \cdot \hat{\mathbf{p}} + \frac{e^2}{2mc} \hat{\mathbf{A}}_s(\hat{\mathbf{r}}) \cdot \hat{\mathbf{A}}_s(\hat{\mathbf{r}}) \right], \quad (\text{B5c})$$

with $V_{ne}^B(\mathbf{r} - \mathbf{r}_{0,B}) \otimes \mathbb{1}$ the potential-energy interaction between the incident electron and the nuclear charge distribution of atom B , and $\hat{\mathbf{V}}_{1,2}(\mathbf{r}, \mathbf{r}')$ the potential-energy interaction between the incident and the target electron. The second term in Eq. (B5a), proportional to $\langle \Phi_{\gamma_a^A}^A | \Phi_{\gamma_b^B}^B \rangle \langle \Phi_{\gamma_b^B}^B | \Phi_{\gamma_a^A}^A \rangle$, arises from the antisymmetriza-

tion of the two-electron state vector in Eq. (B2d) and may not vanish due to the overlap between the scattering states of A and the bound states of B .

After using Eqs. (B5a), (B5b), (B1), and carrying out some straightforward algebra, the expression for the expansion coefficients can be recast into the form

$$S_{\gamma_a^A, \gamma_b^B}^{(k+1)}(\mathbf{n}'; t) = C_{[E]}^{(k+1)}(\gamma_a^A, \gamma_b^B, \mathbf{n}'; t) + C_{[V_B]}^{(k+1)}(\gamma_a^A, \gamma_b^B, \mathbf{n}'; t) + C_{[V_{AB}]}^{(k+1)}(\gamma_a^A, \gamma_b^B, \mathbf{n}'; t) \\ + C_{[h\nu]}^{(k+1)}(\gamma_a^A, \gamma_b^B, \mathbf{n}'; t) + C_{[X]}^{(k+1)}(\gamma_a^A, \gamma_b^B, \mathbf{n}'; t). \quad (\text{B5d})$$

4. Coherent electron-impact dynamics

Defining $\gamma' \equiv (\gamma_a^A, \gamma_b^B)$, the first term in Eq. (B5d),

$$C_{[E]}^{(k+1)}(\gamma', \mathbf{n}'; t) = ie \sum_{\mu_0, \gamma_a^A} \langle \Phi_{\gamma_a^A}^A | \hat{\mathbf{r}}_{\mu_0} f_{\Omega_A}(\mathbf{r}) | \Phi_{\gamma_a^A}^A \rangle \quad (\text{B6}) \\ \times \int_{-\infty}^t S_{\gamma_a^A, \gamma_b^B}^{(k)}(\mathbf{n}'; t') e^{i(\epsilon_{\gamma_a^A}^A - \epsilon_{\gamma_a^A}^A)t'} E_{\mu_0}(t') dt',$$

accounts for the correction to the expansion coefficients due to the classical field defined in Eq. (A2). The second term,

$$C_{[V_B]}^{(k+1)}(\gamma', \mathbf{n}'; t) = -i \sum_{\gamma_a^A} \langle \Phi_{\gamma_a^A}^A | \hat{\mathbf{V}}_{ne}(\mathbf{r} - r_{0,B}) | \Phi_{\gamma_a^A}^A \rangle \\ \times \int_{-\infty}^t S_{\gamma_a^A, \gamma_b^B}^{(k)}(\mathbf{n}'; t') e^{i(\epsilon_{\gamma_a^A}^A - \epsilon_{\gamma_a^A}^A)t'} dt', \quad (\text{B7})$$

accounts for the correction to the scattering component γ_a^A of the expansion coefficients due to the potential-energy interaction between the incoming electron and the nuclear charge density at $r_{0,B}$ while leaving the component γ_b^B and the photon field unchanged. Next,

$$C_{[V_{AB}]}^{(k+1)}(\gamma', \mathbf{n}'; t) = -i \sum_{\gamma_a^A, \gamma_b^B} \langle \Phi_{\gamma_a^A}^A \Phi_{\gamma_b^B}^B | \hat{\mathbf{V}}_{1,2}(\mathbf{r}, \mathbf{r}') | \Phi_{\gamma_a^A}^A \Phi_{\gamma_b^B}^B \rangle \\ \times \int_{-\infty}^t S_{\gamma_a^A, \gamma_b^B}^{(k)}(\mathbf{n}'; t') e^{i\varphi(\gamma', \gamma_a^A, \gamma_b^B)t'} dt', \quad (\text{B8})$$

where $\varphi(\gamma', \gamma_a^A, \gamma_b^B) \equiv \epsilon_{\gamma_a^A}^A + \epsilon_{\gamma_b^B}^B - \epsilon_{\gamma_a^A}^A - \epsilon_{\gamma_b^B}^B$, accounts for the interaction between the incoming electron and the electron initially in atom B . More precisely, Eq. (B8)

accounts for the elastic and inelastic excitation of atom B triggered by the incident wave packet. It describes, to lowest order, the scattering of an initial continuum-state component along $|\Phi_{\gamma_a^A}^A\rangle$ to $|\Phi_{\gamma_a^A}^A\rangle$, leading to excitation of atom B from $|\Phi_{\gamma_b^B}^B\rangle$ to $|\Phi_{\gamma_b^B}^B\rangle$ without change in the distribution of photon modes.

5. Single photons and sequentially/simultaneously emitted (absorbed) photon pairs

a. One-photon exchange

De-excitation of atom B following the excitation triggers the dynamics of photon emission (absorption) dictated by the fourth term in Eq. (B5d). The latter can be split according to the net number of exchanged photons as

$$C_{[h\nu]}^{(k+1)}(\gamma_a^A, \gamma_b^B, \mathbf{n}'; t) = -i \kappa_{1ph} C_{[1ph]}^{(k+1)}(\gamma', \mathbf{n}'; t) \\ - i \kappa_{2ph} C_{[2ph]}^{(k+1)}(\gamma', \mathbf{n}'; t), \quad (\text{B9})$$

with $\kappa_{1ph} = -e/mc$ and $\kappa_{2ph} = e^2/2mc$. The first (second) term in Eq. (B9) describes the exchange of one (two) photons. The first term arises from the contribution $\propto \hat{\mathbf{A}}_s(\mathbf{r}) \cdot \hat{\mathbf{p}}$ in Eq. (B5c). It can be written as

$$C_{[1ph]}^{(k+1)}(\gamma', \mathbf{n}'; t) = W_{[abs]}^{(k+1)}(\gamma', \mathbf{n}'; t) + W_{[em]}^{(k+1)}(\gamma', \mathbf{n}'; t). \quad (\text{B10})$$

The two parts in Eq. (B10) dictate the absorption and emission of one net photon according to

$$W_{[abs]}^{(k+1)}(\gamma', \mathbf{n}'; t) = \sum_{\gamma_b^B} \sum_{q \in \Omega_\gamma} A_q \sqrt{n'_q + 1} \langle \Phi_{\gamma_b^B}^B | e^{i\mathbf{k}_q \cdot \mathbf{r}} \hat{\mathbf{p}} | \Phi_{\gamma_b^B}^B \rangle \cdot \epsilon_q \int_{-\infty}^t S_{\gamma_a^A, \gamma_b^B}^{(k)}(\mathbf{n}' + \mathbf{1}_q; t') e^{i(\epsilon_{\gamma_b^B}^B - \epsilon_{\gamma_b^B}^B - \hbar\omega_q)t'} dt', \quad (\text{B11a})$$

$$W_{[em]}^{(k+1)}(\gamma', \mathbf{n}'; t) = \sum_{\gamma_b^B} \sum_{q \in \Omega_\gamma} A_q \sqrt{n'_q} \langle \Phi_{\gamma_b^B}^B | e^{-i\mathbf{k}_q \cdot \mathbf{r}} \hat{\mathbf{p}} | \Phi_{\gamma_b^B}^B \rangle \cdot \epsilon_q \int_{-\infty}^t S_{\gamma_a^A, \gamma_b^B}^{(k)}(\mathbf{n}' - \mathbf{1}_q; t') e^{i(\epsilon_{\gamma_b^B}^B - \epsilon_{\gamma_b^B}^B + \hbar\omega_q)t'} dt'. \quad (\text{B11b})$$

Here we used the convention of Eq. (B4) and defined

$A_q = \sqrt{\hbar/2\omega_q\epsilon_0 V_0}$. The photon mode labelled as q is

defined by the momentum, $\hbar \mathbf{k}_q$, and polarization, $\boldsymbol{\epsilon}_q$, of the emitted (absorbed) photon. Emission (absorption) of a photon in mode q yields de-excitation (excitation) of atom B from $|\Phi_{\gamma_b}^B\rangle$ to $|\Phi_{\gamma'_b}^B\rangle$. For entangled photon pairs sequentially emitted in a radiative photon cascade process, the largest contributing term is given by Eq. (B11b), although the dynamics of photoemission may also be affected by additional terms describing absorption and emission involving two-photon exchange processes.

b. Two-photon exchange

The coefficient $C_{[2ph]}^{(k+1)}(\gamma', \mathbf{n}'; t)$ in Eq. (B9) arises from the term proportional to $\hat{\mathbf{A}}_s(\mathbf{r}) \cdot \hat{\mathbf{A}}_s(\mathbf{r})$ in Eq. (B5c). It describes real and virtual two-photon emission (absorption) in the same or different modes with effective two or zero net photon exchange processes between atom B and the photon field. Compared to its counterpart proportional to κ_{1ph} in Eq. (B9), this term is $\propto e^2$. Consequently, it

provides a weaker contribution to one-step cascade processes. However, it must be taken into account for radiative processes involving two or more optical cascades, as the multiplying factors appearing in powers of e for both terms may become commensurate. We define this term according to whether or not the exchanged photons are in the same or different modes, namely

$$C_{[2ph]}^{(k+1)}(\gamma', \mathbf{n}'; t) = P^{(k+1)}(\gamma', \mathbf{n}'; t) + Q^{(k+1)}(\gamma', \mathbf{n}'; t). \quad (\text{B12})$$

The first (second) term in Eq. (B12) describes the exchange of two photons in the same (or different) mode(s). The first term in Eq. (B12) may be decomposed as

$$P^{(k+1)}(\gamma', \mathbf{n}'; t) = P_{[em,em]}^{(k+1)}(\gamma', \mathbf{n}'; t) + P_{[abs,abs]}^{(k+1)}(\gamma', \mathbf{n}'; t) + P_{[em,abs]}^{(k+1)}(\gamma', \mathbf{n}'; t), \quad (\text{B13})$$

where we have defined (using $|\Phi_{\gamma_b}^B\rangle \equiv |\Phi_{\gamma_b}^B\rangle$),

$$P_{[abs,abs]}^{(k+1)}(\gamma', \mathbf{n}'; t) = \sum_{\gamma_b^B} \sum_{q \in \Omega_\gamma} A_q A_q \langle \Phi_{\gamma_b'}^B | e^{2i\mathbf{k}_q \cdot \mathbf{r}} | \Phi_{\gamma_b}^B \rangle \sqrt{n_q + 1} \sqrt{n_q + 2} \int_{-\infty}^t S_{\gamma'_A, \gamma_b^B}^{(k)}(\mathbf{n}' + \mathbf{2}_q; t') e^{i(\epsilon_{\gamma_b'}^B - \epsilon_{\gamma_b}^B - 2\hbar\omega_q)t'} dt'; \quad (\text{B14a})$$

$$P_{[em,em]}^{(k+1)}(\gamma', \mathbf{n}'; t) = \sum_{\gamma_b^B} \sum_{q \in \Omega_\gamma} A_q A_q \langle \Phi_{\gamma_b'}^B | e^{-2i\mathbf{k}_q \cdot \mathbf{r}} | \Phi_{\gamma_b}^B \rangle \sqrt{n'_q - 1} \sqrt{n'_q} \int_{-\infty}^t S_{\gamma'_A, \gamma_b^B}^{(k)}(\mathbf{n}' - \mathbf{2}_q; t') e^{i(\epsilon_{\gamma_b'}^B - \epsilon_{\gamma_b}^B + 2\hbar\omega_q)t'} dt'; \quad (\text{B14b})$$

$$P_{[em,abs]}^{(k+1)}(\gamma', \mathbf{n}'; t) = \sum_{q \in \Omega_\gamma} A_q A_q (2n'_q + 1) \int_{-\infty}^t S_{\gamma'_A, \gamma_b^B}^{(k)}(\mathbf{n}'; t') dt'. \quad (\text{B14c})$$

Equation (B14a) describes the absorption of two photons in the same mode q and subsequent excitation of atom B from $|\Phi_{\gamma_b}^B\rangle$ to $|\Phi_{\gamma_b'}^B\rangle$, leaving the scattered photoelectron unaffected if two photons in the same mode q are present in the field at the previous iteration step (k), and if the state $|\Phi_{\gamma_b}^B\rangle$ is populated. The distribution of modes then goes from $\mathbf{n}' + \mathbf{2}_q$ to \mathbf{n}'_q photons in mode q , i.e., compare the terms $S_{\gamma'_A, \gamma_b^B}^{(k)}(\mathbf{n}' + \mathbf{2}_q; t')$ (uncorrected) and $P_{[em,em]}^{(k+1)}(\gamma', \mathbf{n}'; t)$ (corrected).

Next, Eq. (B14b) accounts for the emission of two photons in the same mode q . For $k_q r \ll 1$, the description of excitation (de-excitation) induced by simultaneous two-photon absorption (emission) requires both terms to be

treated beyond the dipole approximation. Note that emission and absorption of photons may occur without excitation (de-excitation), even in the dipole approximation. Simultaneous emission of a photon in mode q and absorption of a photon in the same mode with no electron dynamics involved is described by Eq. (B14c).

Finally, the second term in Eq. (B12), describing the simultaneous exchange of two photons in different modes, reads

$$Q^{(k+1)}(\gamma', \mathbf{n}'; t) = Q_{[abs,abs]}^{(k+1)}(\gamma', \mathbf{n}'; t) + Q_{[em,em]}^{(k+1)}(\gamma', \mathbf{n}'; t) + Q_{[em,abs]}^{(k+1)}(\gamma', \mathbf{n}'; t), \quad (\text{B15})$$

where, in analogy with Eq. (B14), we have defined

$$Q_{[abs,abs]}^{(k+1)}(\gamma', \mathbf{n}'; t) = \sum_{\gamma_b^B} \sum_{\substack{p, q \in \Omega \\ p \neq q}} A_q^p (n'_p + 1, n'_q + 1) \langle \Phi_{\gamma_b'}^B | e^{i(\mathbf{k}_p + \mathbf{k}_q) \cdot \mathbf{r}} | \Phi_{\gamma_b}^B \rangle \int_{-\infty}^t S_{\gamma'_A, \gamma_b^B}^{(k)}(\mathbf{n}' + \mathbf{1}_p + \mathbf{1}_q; t') e^{i[\epsilon_{\gamma_b'}^B - \epsilon_{\gamma_b}^B - \hbar(\omega_p + \omega_q)]t'} dt'; \quad (\text{B16a})$$

$$Q_{[em,em]}^{(k+1)}(\gamma', \mathbf{n}'; t) = \sum_{\gamma_b^B} \sum_{\substack{p,q \in \Omega \\ p \neq q}} A_q^p(n'_p, n'_q) \langle \Phi_{\gamma_b^B}^B | e^{-i(\mathbf{k}_p + \mathbf{k}_q) \cdot \hat{\mathbf{r}}} | \Phi_{\gamma_b^B}^B \rangle \int_{-\infty}^t S_{\gamma_a^A, \gamma_b^B}^{(k)}(\mathbf{n}' + \mathbf{1}_p + \mathbf{1}_q; t') e^{i[\epsilon_{\gamma_b^B}^B - \epsilon_{\gamma_b^B}^B + \hbar(\omega_p + \omega_q)]t'} dt'; \quad (\text{B16b})$$

$$Q_{[abs,em]}^{(k+1)}(\gamma', \mathbf{n}'; t) = \sum_{\gamma_b^B} \sum_{\substack{p,q \in \Omega \\ p \neq q}} A_q^p(n'_p + 1, n'_q) \langle \Phi_{\gamma_b^B}^B | e^{i(\mathbf{k}_p - \mathbf{k}_q) \cdot \hat{\mathbf{r}}} | \Phi_{\gamma_b^B}^B \rangle \int_{-\infty}^t S_{\gamma_a^A, \gamma_b^B}^{(k)}(\mathbf{n}' + \mathbf{1}_p + \mathbf{1}_q; t') e^{i[\epsilon_{\gamma_b^B}^B - \epsilon_{\gamma_b^B}^B + \hbar(\omega_p - \omega_q)]t'} dt', \quad (\text{B16c})$$

with $A_q^p(n'_p, n'_q) = A_p A_q \sqrt{n'_p} \sqrt{n'_q} (\mathbf{e}_p \cdot \mathbf{e}_q)$. Equation (B16a) accounts for the simultaneous absorption of two photons in different modes, while Eq. (B16b) describes the simultaneous emission of two photons in different modes. Finally, Eq. (B16c) accounts for the exchange of photon pairs without a net change in the photon number: it describes the simultaneous absorption and emission of one photon in different modes. The matrix elements and angular distributions involving simultaneously emitted (absorbed) photon pairs are evaluated following the prescription given in Sec. C 2 b.

For the photon wavelengths considered in this work, the contribution due to the term $\hat{\mathbf{A}}_s(\hat{\mathbf{r}}) \cdot \hat{\mathbf{A}}_s(\hat{\mathbf{r}})$ driving *simultaneous photon pair emission* via optical de-excitation is expected to be less important compared to the case of *sequential photon pair emission* mediated by the term $\hat{\mathbf{A}}_s(\hat{\mathbf{r}}) \cdot \hat{\mathbf{p}}$, since the matrix elements corre-

sponding to the former would vanish in the dipole approximation. It is worth mentioning that Eq. (B11b), or more specifically, a two-step sequential application of Eq. (B11b), provides the leading contribution to the emission of photon pairs with energies $\hbar\nu_1$ and $\hbar\nu_2$: the correlated photon pair originates from sequential emission from the target atom B , following the de-excitation pathways depicted in Fig. 1(c).

6. Exchange term $C_{[X]}^{(k+1)}(\gamma_a^A, \gamma_b^B, \mathbf{n}'; t)$

Finally, proper antisymmetrization of the two-electron wave function is ensured by the last term in Eq. (B5d): $C_{[X]}^{(k+1)}(\gamma_a^A, \gamma_b^B, \mathbf{n}'; t)$. The latter updates the expansion coefficients to ensure the required exchange symmetry via the iterative correction

$$\begin{aligned} C_{[X]}^{(k+1)}(\gamma_a^A, \gamma_b^B, \mathbf{n}'; t) &= i \sum_{\gamma_a^A, \gamma_b^B} \langle \Phi_{\gamma_a^A}^A | \hat{\mathbf{V}}_{ne}(\hat{\mathbf{r}} - r_{0,B}) | \Phi_{\gamma_b^B}^B \rangle \langle \Phi_{\gamma_b^B}^B | \Phi_{\gamma_a^A}^A \rangle \int_{-\infty}^t S_{\gamma_a^A, \gamma_b^B}^{(k)}(\mathbf{n}'; t') e^{i(\epsilon_{\gamma_a^A}^A + \epsilon_{\gamma_b^B}^B - \epsilon_{\gamma_a^A}^A - \epsilon_{\gamma_b^B}^B)t'} dt' \\ &+ i \sum_{\gamma_a^A, \gamma_b^B} \langle \Phi_{\gamma_a^A}^A \Phi_{\gamma_b^B}^A | \hat{\mathbf{V}}_{12}(\hat{\mathbf{r}}, \hat{\mathbf{r}}') | \Phi_{\gamma_b^B}^B \Phi_{\gamma_a^A}^A \rangle \int_{-\infty}^t S_{\gamma_a^A, \gamma_b^B}^{(k)}(\mathbf{n}'; t') e^{i(\epsilon_{\gamma_a^A}^A + \epsilon_{\gamma_b^B}^B - \epsilon_{\gamma_a^A}^A - \epsilon_{\gamma_b^B}^B)t'} dt' \\ &- \sum_{\gamma_a^A} \underline{\underline{C}}_{[h\nu]}^{(k+1)}(\gamma_a^A, \gamma_b^B, \mathbf{n}'; t) + \sum_{\gamma_a^A, \gamma_b^B} \mathcal{O}_{\gamma_a^A, \gamma_b^B}^{\gamma_a^A, \gamma_b^B} \left[S_{\gamma_a^A, \gamma_b^B}^{(k)}(\mathbf{n}'; t') e^{i(\epsilon_{\gamma_a^A}^A + \epsilon_{\gamma_b^B}^B - \epsilon_{\gamma_a^A}^A - \epsilon_{\gamma_b^B}^B)t'} \right]_{-\infty}^t, \quad (\text{B17a}) \end{aligned}$$

where the overlap matrix, already appearing in Eq. (B5a), reads

$$\mathcal{O}_{\gamma_a^A, \gamma_b^B}^{\gamma_a^A, \gamma_b^B} = \langle \Phi_{\gamma_a^A}^A | \Phi_{\gamma_b^B}^B \rangle \langle \Phi_{\gamma_b^B}^B | \Phi_{\gamma_a^A}^A \rangle. \quad (\text{B17b})$$

The double underline in the third term in Eq. (B17a) indicates that the expressions $(\epsilon_{\gamma_b^B}^B - \epsilon_{\gamma_b^B}^B)$ as well as all transition matrix elements of the form $\langle \Phi_{\gamma_b^B}^B | \mathcal{T} | \Phi_{\gamma_b^B}^B \rangle$ appearing through Eqs. (B11a)-(B16c) must be replaced with $(\epsilon_{\gamma_a^A}^A + \epsilon_{\gamma_b^B}^B - \epsilon_{\gamma_a^A}^A + \epsilon_{\gamma_b^B}^B)$ and $\langle \Phi_{\gamma_b^B}^B | \mathcal{T} | \Phi_{\gamma_a^A}^A \rangle \langle \Phi_{\gamma_a^A}^A | \Phi_{\gamma_b^B}^B \rangle$, respectively. Note that the classical field does not contribute to the exchange term because of $f_{\Omega_A}(r)$ and the localized character of \mathcal{H}_B , i.e., the expansion coefficients vanish for the continuum states of atom B : ionization of atom B by electron impact is not considered.

Appendix C: Polarization states and propagation direction of emitted (absorbed) photons

1. Transversality condition and polarization components

a. General scheme

Throughout the text, we used the shorthand notation

$$\boldsymbol{\sigma}_j \equiv (\sigma_{ja}, \sigma_{jb}), \quad (\text{C1})$$

when referring to the indices of the two mutually orthogonal polarization components $\hat{\epsilon}_{\sigma_{ja}}$ and $\hat{\epsilon}_{\sigma_{jb}}$ satisfying the transversality conditions

$$\hat{\epsilon}_{\sigma_j} \cdot \mathbf{k}_j = 0. \quad (\text{C2})$$

Within this convention, summation over the indices σ_j , e.g., in Eq. (B2d), implies summation over their components in Eq. (C1) for each momentum $\hbar\mathbf{k}_j$. To construct ϵ_{σ_j} , or equivalently $\epsilon_{\sigma_{ja}}$ and $\epsilon_{\sigma_{jb}}$ satisfying Eq. (C2), we write \mathbf{k}_j in polar coordinates,

$$\mathbf{k}_j = \sqrt{\frac{4\pi}{3}} \left(\frac{\omega_j}{c} \right) \sum_{q=0,\pm 1} Y_q^1(\theta_{k_j}, \phi_{k_j}) \hat{\mathbf{e}}_q^*, \quad (\text{C3})$$

with $Y_q^1(\theta_{k_j}, \phi_{k_j})$ as the spherical harmonic for the propagation direction of the mode (\mathbf{k}_j, σ_j) and $\hat{\mathbf{e}}_q$ denoting the covariant spherical unit vectors $\mathbf{e}_{-1} = (\mathbf{e}_x - i\mathbf{e}_y)/\sqrt{2}$, $\mathbf{e}_{+1} = -(\mathbf{e}_x + i\mathbf{e}_y)/\sqrt{2}$, and $\mathbf{e}_0 = \mathbf{e}_z$. We then construct the orthogonal triad of unit vectors $(\mathbf{k}_j/|\mathbf{k}_j|, \epsilon_{\sigma_{jq}}, \epsilon_{\sigma_{jq}})$ as

$$\begin{aligned} \hat{\epsilon}_{\sigma_{ja}} &= \frac{\mathbf{k}_j \times \hat{\mathbf{e}}_0}{|\mathbf{k}_j \times \hat{\mathbf{e}}_0|} = \frac{1}{\sqrt{2}} \left[i \cos(\theta_{k_j}) - \sin(\phi_{k_j}) \right] \mathbf{e}_{+1} \\ &\quad + \frac{1}{\sqrt{2}} \left[i \cos(\theta_{k_j}) + \sin(\phi_{k_j}) \right] \mathbf{e}_{-1}, \quad (\text{C4}) \end{aligned}$$

for the first polarization component and

$$\begin{aligned} \hat{\epsilon}_{\sigma_{jb}} &= \frac{\mathbf{k}_j \times \hat{\epsilon}_{\sigma_{ja}}}{|\mathbf{k}_j \times \hat{\epsilon}_{\sigma_{ja}}|} \\ &= -\frac{1}{\sqrt{2}} \left[i \sin(\phi_{k_j}) \cos(\theta_{k_j}) + \cos(\phi_{k_j}) \cos(\theta_{k_j}) \right] \mathbf{e}_{+1} \\ &\quad - \frac{1}{\sqrt{2}} \left[i \sin(\phi_{k_j}) \cos(\theta_{k_j}) - \cos(\phi_{k_j}) \cos(\theta_{k_j}) \right] \mathbf{e}_{-1} \\ &\quad - \sin(\theta_{k_j}) \mathbf{e}_0, \quad (\text{C5}) \end{aligned}$$

for the second polarization component, with (\times) denoting the vector cross product. They both fulfill the transversality condition $\hat{\epsilon}_{\sigma_j} \cdot \mathbf{k}_j = 0$.

In cartesian coordinates, $[\hat{\mathbf{e}}_x, \hat{\mathbf{e}}_y, \hat{\mathbf{e}}_z]$, $\epsilon_{\sigma_{ja}}$ and $\epsilon_{\sigma_{jb}}$ are

$$\hat{\epsilon}_{\sigma_{ja}} \equiv \begin{bmatrix} \sin(\phi_{k_j}) \\ -\cos(\phi_{k_j}) \\ 0 \end{bmatrix}; \quad \hat{\epsilon}_{\sigma_{jb}} \equiv \begin{bmatrix} \cos(\phi_{k_j}) \cos(\theta_{k_j}) \\ -\sin(\phi_{k_j}) \cos(\theta_{k_j}) \\ -\sin(\theta_{k_j}) \end{bmatrix}. \quad (\text{C6})$$

b. Application to the correlated photodetection scheme

Following the photodetection scheme of Fig. 2(b), a photon in mode (2) is detected at the fixed angles $\theta_{k_2} = \pi/2$ and $\phi_{k_2} = -\pi/2$. This gives, according to Eq. (C6),

$\epsilon_{\sigma_{2a}} = [-1, 0, 0]$ and $\epsilon_{\sigma_{2b}} = [0, 0, -1]$. The first detector measures the photon with energy $\hbar\nu_2$ with polarization component along $\epsilon_{\sigma_{2b}}$, i.e., along $\hat{\mathbf{z}}$.

A second detector detects the photon with energy $\hbar\nu_1$ at fixed $\phi_{k_1} = \pi/2$, but it is free to move and hence scan along θ_{k_1} . According to Eq. (C6), this corresponds to $\epsilon_{\sigma_{1a}} = [1, 0, 0]$ and $\epsilon_{\sigma_{1b}} = [0, -\cos(\theta_{k_1}), -\sin(\theta_{k_1})]$. The second detector measures the correlated photon pair with energy $\hbar\nu_1$ with polarization component along $\epsilon_{\sigma_{1b}}$ as it scans along θ_{k_1} .

2. Angular distributions and transition matrix elements

a. Angular distributions of single photons and sequentially emitted (absorbed) photon pairs

The directions of propagation of the emitted (absorbed) photons are evaluated by means of a multipole expansion of the exponential terms, $\exp(ikr)$, which appear in the matrix elements of the expansion coefficients defined throughout Sec. B5. Specifically,

$$e^{\pm i\mathbf{k}_j \cdot \mathbf{r}} = 4\pi \sum_{\lambda, \mu} (\pm i)^\lambda j_\lambda(k_j r) Y_\mu^\lambda(\theta_r, \phi_r) Y_\mu^{\lambda*}(\theta_{k_j}, \phi_{k_j}), \quad (\text{C7})$$

where $j_\lambda(k_j r)$ denotes a spherical Bessel function. For the photon energies considered in this work, the wavelengths defining the modes emitted and absorbed during the propagation of the expansion coefficients are several orders of magnitude larger than the extension of the most diffuse bound state of the target atom B . The Bessel functions can therefore be approximated by

$$j_\lambda(k_j r) \approx (k_j r)^\lambda / (2\lambda + 1)!!, \quad (\text{C8})$$

since $k_j r \ll 1$. This allows us to obtain the transition matrix elements as a power series in r^λ . Following this prescription, the matrix elements defined in Eqs. (B11a) and (B11b) are given by

$$\begin{aligned} \langle \Phi_{\gamma'_B}^B | e^{\pm i\mathbf{k}_j \cdot \mathbf{r}} \hat{\mathbf{p}}_{\mu_0} | \Phi_{\gamma_B}^B \rangle &= \sum_{\lambda, \mu} \langle \Phi_{\gamma'_B}^B | \mathcal{D}_{\mu, \mu_0}^{[\lambda, \pm]}(k_j) | \Phi_{\gamma_B}^B \rangle \\ &\quad \times Y_\mu^{\lambda*}(\Omega_{k_j}), \quad (\text{C9a}) \end{aligned}$$

with $\Omega_{k_j} \equiv (\theta_{k_j}, \phi_{k_j})$. The multipole coefficients are obtained by standard angular-momentum techniques as

$$\begin{aligned}
\langle \Phi_{\gamma_b^B}^B | \mathcal{D}_{\mu, \mu_0}^{[\lambda, \pm]}(k_j) | \Phi_{\gamma_b^B}^B \rangle &= C \frac{(\pm i)^\lambda (k_j)^\lambda}{(2\lambda + 1)!!} (-1)^{l' + m'} \sum_{q=|l' - \lambda|}^{l' + \lambda} \left[\frac{(2l' + 1)(2\lambda + 1)}{1/(2q + 1)} \right]^{\frac{1}{2}} \begin{pmatrix} l' & \lambda & q \\ -m' & \mu & m + \mu_0 \end{pmatrix} \begin{pmatrix} l' & \lambda & q \\ 0 & 0 & 0 \end{pmatrix} \delta_{m' - \mu, m + \mu_0} \\
&\times \begin{cases} \int_0^{+\infty} r^{\lambda+2} f_{n', l'}(r) \left(\frac{\partial}{\partial r} - \frac{l}{r} \right) f_{n, l}(r) dr \left[\left(\frac{l+1}{2l+3} \right)^{\frac{1}{2}} (-1)^{l-1+m+\mu_0} \begin{pmatrix} l & 1 & l+1 \\ m & \mu_0 & -m - \mu_0 \end{pmatrix} \right] \delta_{q, l+1} \\ - \int_0^{+\infty} r^{\lambda+2} f_{n', l'}(r) \left(\frac{\partial}{\partial r} + \frac{l}{r} \right) f_{n, l}(r) dr \left[\left(\frac{l}{2l-1} \right)^{\frac{1}{2}} (-1)^{l-1+m+\mu_0} \begin{pmatrix} l & 1 & l-1 \\ m & \mu_0 & m + \mu_0 \end{pmatrix} \right] \delta_{q, l-1} \end{cases}
\end{aligned} \tag{C9b}$$

with $C = -i\hbar\sqrt{36\pi}$. Furthermore, (n', l', m') and (n, l, m) denote the quantum numbers corresponding to $\gamma_b^{l'B}$ and γ_b^B , while $f_{n', l'}(r)$ and $f_{n, l}(r)$ are the radial components of the orbital wavefunctions $\langle \mathbf{r} | \Phi_{\gamma_b^B}^B \rangle$ and $\langle \mathbf{r} | \Phi_{\gamma_b^{l'B}}^B \rangle$, respectively.

b. Angular distributions of simultaneously emitted (absorbed) photon pairs

Analogously, the matrix elements describing simultaneous two-photon exchange, i.e., emission ($s = -1$) or absorption ($s = +1$) of a photon in mode q_s with momentum $\hbar \mathbf{k}_s$ and emission ($s' = -1$) or absorption ($s' = +1$)

of another photon in mode $q_{s'}$ with momentum $\hbar \mathbf{k}_{s'}$, such as those appearing in Eqs. (B16), are obtained according to the multipole expansion involving the product of two spherical harmonics. Specifically,

$$\begin{aligned}
\langle \Phi_{\gamma_b^B}^B | e^{i(s\mathbf{k}_s + s'\mathbf{k}_{s'}) \cdot \hat{\mathbf{r}}} | \Phi_{\gamma_b^B}^B \rangle &= \sum_{\substack{\lambda_{s'}, \mu_{s'} \\ \lambda_s, \mu_s}} \langle \Phi_{\gamma_b^B}^B | \mathcal{O}_{\mu_s, \mu_{s'}}^{[\lambda_s, \lambda_{s'}]}(\mathbf{v}_s^{s'}) | \Phi_{\gamma_b^B}^B \rangle \\
&\times Y_{\mu_s}^{\lambda_s*}(\Omega_{k_s}) Y_{\mu_{s'}}^{\lambda_{s'}*}(\Omega_{k_{s'}}),
\end{aligned} \tag{C10a}$$

where we have defined $\mathbf{v}_s^{s'} \equiv [k_s, s, k_{s'}, s']$. The coefficients are again obtained after straightforward angular-momentum algebra. The result is

$$\begin{aligned}
\langle \Phi_{\gamma_b^B}^B | \mathcal{O}_{\mu_s, \mu_{s'}}^{[\lambda_s, \lambda_{s'}]}(\mathbf{v}_s^{s'}) | \Phi_{\gamma_b^B}^B \rangle &= (4\pi)^2 \frac{(is)^{\lambda_s} (is')^{\lambda_{s'}}}{(2\lambda_s + 1)!!} \frac{(k_s k_{s'})^{\lambda_s + \lambda_{s'}}}{(2\lambda_{s'} + 1)!!} (-1)^{l' + m' - \mu_s - \mu_{s'}} \int_0^{+\infty} f_{n', l'}(r) r^{\lambda_s + \lambda_{s'} + 2} f_{n, l}(r) dr \\
&\times \sum_{\Lambda=|\lambda_s - \lambda_{s'}|}^{\lambda_s + \lambda_{s'}} (-1)^\Lambda \begin{pmatrix} \lambda_s & \lambda_{s'} & \Lambda \\ \mu_s & \mu_{s'} & -\mu_s - \mu_{s'} \end{pmatrix} \begin{pmatrix} \lambda_s & \lambda_{s'} & \Lambda \\ 0 & 0 & 0 \end{pmatrix} \begin{pmatrix} l' & \Lambda & l \\ -m' & \mu_s + \mu_{s'} & m \end{pmatrix} \begin{pmatrix} l' & \Lambda & l \\ 0 & 0 & 0 \end{pmatrix} \\
&\times \left[\frac{(2\lambda_s + 1)(2\lambda_{s'} + 1)}{4\pi/(2\Lambda + 1)} \right]^{\frac{1}{2}} \delta_{m' - m, \mu_s + \mu_{s'}}.
\end{aligned} \tag{C10b}$$

-
- [1] D. Tannor and S. Rice, *J. Chem. Phys.* **83**, 5013 (1985).
 - [2] M. Shapiro and P. Brumer, *Quantum control of molecular processes* (John Wiley & Sons, 2012).
 - [3] M. Shapiro and P. Brumer, *Rep. Prog. Phys.* **66**, 859 (2003).
 - [4] H. Eichmann, A. Egbert, S. Nolte, C. Momma, B. Wellegehausen, W. Becker, S. Long, and J. K. McIver, *Phys. Rev. A* **51**, R3414 (1995).
 - [5] D. B. Milošević, W. Becker, and R. Kopold, *Phys. Rev. A* **61**, 063403 (2000).
 - [6] M. Wollenhaupt, A. Assion, D. Liese, C. Sarpe-Tudoran, T. Baumert, S. Zamith, M. A. Bouchene, B. Girard, A. Flettner, U. Weichmann, and G. Gerber, *Phys. Rev. Lett.* **89**, 173001 (2002).
 - [7] S. Kerbstadt, K. Eickhoff, T. Bayer, and M. Wollenhaupt, *Advances in Physics: X* **4**, 1672583 (2019).
 - [8] Y.-Y. Yin, C. Chen, D. S. Elliott, and A. V. Smith, *Phys. Rev. Lett.* **69**, 2353 (1992).
 - [9] K.-J. Yuan and A. D. Bandrauk, *J. Phys. B* **49**, 065601 (2016).
 - [10] A. N. Grum-Grzhimailo, E. V. Gryzlova, E. I. Staroselskaya, J. Venzke, and K. Bartschat, *Phys. Rev. A* **91**, 063418 (2015).
 - [11] A. N. Grum-Grzhimailo, E. V. Gryzlova, E. I. Staroselskaya, S. I. Strakhova, J. Venzke, N. Douguet, and K. Bartschat, *Journal of Physics: Conference Series* **635**,

- 012008 (2015).
- [12] N. Douguet, A. N. Grum-Grzhimailo, E. V. Gryzlova, E. I. Staroselskaya, J. Venzke, and K. Bartschat, *Phys. Rev. A* **93**, 033402 (2016).
 - [13] E. V. Gryzlova, A. N. Grum-Grzhimailo, E. I. Staroselskaya, N. Douguet, and K. Bartschat, *Phys. Rev. A* **97**, 013420 (2018).
 - [14] P. V. Demekhin, A. N. Artemyev, A. Kastner, and T. Baumert, *Phys. Rev. Lett.* **121**, 253201 (2018).
 - [15] R. E. Goetz, C. P. Koch, and L. Greenman, *Phys. Rev. Lett.* **122**, 013204 (2019).
 - [16] M. Wollenhaupt, C. Lux, M. Krug, and T. Baumert, *ChemPhysChem* **14**, 1297 (2013).
 - [17] C.-Y. Lu, D. E. Browne, T. Yang, and J.-W. Pan, *Phys. Rev. Lett.* **99**, 250504 (2007).
 - [18] X.-Q. Zhou, P. Kalasuwan, T. C. Ralph, and J. L. O'Brien, *Nature photonics* **7**, 223 (2013).
 - [19] P. G. Kwiat, K. Mattle, H. Weinfurter, A. Zeilinger, A. V. Sergienko, and Y. Shih, *Phys. Rev. Lett.* **75**, 4337 (1995).
 - [20] X. Guo, C.-I. Zou, C. Schuck, H. Jung, R. Cheng, and H. X. Tang, *Light: Science & Applications* **6**, e16249 (2017).
 - [21] M. B. Nasr, B. E. A. Saleh, A. V. Sergienko, and M. C. Teich, *Phys. Rev. Lett.* **91**, 083601 (2003).
 - [22] T. Ono, R. Okamoto, and S. Takeuchi, *Nature communications* **4**, 1 (2013).
 - [23] B. E. A. Saleh, B. M. Jost, H.-B. Fei, and M. C. Teich, *Phys. Rev. Lett.* **80**, 3483 (1998).
 - [24] R. de J León-Montiel, J. Svozilík, L. J. Salazar-Serrano, and J. P. Torres, *New J. Phys.* **15**, 053023 (2013).
 - [25] J. Svozilík, J. Peřina, and R. de J. León-Montiel, *J. Opt. Soc. Am. B* **35**, 460 (2018).
 - [26] R. d. J. León-Montiel, J. c. v. Svozilík, J. P. Torres, and A. B. U'Ren, *Phys. Rev. Lett.* **123**, 023601 (2019).
 - [27] F. Schlawin, K. E. Dorfman, and S. Mukamel, *Phys. Rev. A* **93**, 023807 (2016).
 - [28] K. E. Dorfman, F. Schlawin, and S. Mukamel, *Rev. Mod. Phys.* **88**, 045008 (2016).
 - [29] S. Mukamel, K. E. Dorfman, M. Kowalewski, K. Bennett, and F. Schlawin, in *Frontiers in Optics 2017* (Optical Society of America, 2017) p. LTu5F.2.
 - [30] F. Schlawin, *J. Phys. B* **50**, 203001 (2017).
 - [31] F. Schlawin and S. Mukamel, *J. Chem. Phys.* **139**, 244110 (2013).
 - [32] H. Oka, *J. Chem. Phys.* **152**, 044106 (2020).
 - [33] F. Schlawin, K. E. Dorfman, and S. Mukamel, *Acc. Chem. Res.* **51**, 2207 (2018).
 - [34] E. Paspalakis and P. L. Knight, *Phys. Rev. Lett.* **81**, 293 (1998).
 - [35] T. Quang, M. Woldeyohannes, S. John, and G. S. Agarwal, *Phys. Rev. Lett.* **79**, 5238 (1997).
 - [36] F. Ghafoor, S.-Y. Zhu, and M. S. Zubairy, *Phys. Rev. A* **62**, 013811 (2000).
 - [37] X. Sun, B. Zhang, and X. Jiang, *Eur. Phys. J. D* **55**, 699 (2009).
 - [38] L. Hutter, G. Lima, and S. P. Walborn, *Phys. Rev. Lett.* **125**, 193602 (2020).
 - [39] Y. Jeronimo-Moreno and A. B. U'Ren, *Phys. Rev. A* **79**, 033839 (2009).
 - [40] O. Lib, G. Hasson, and Y. Bromberg, *Science Advances* **6** (2020), 10.1126/sciadv.abb6298.
 - [41] V. Weisskopf and E. Wigner, in *Part I: Particles and Fields. Part II: Foundations of Quantum Mechanics* (Springer, 1997) pp. 30–49.
 - [42] O. Zatsarinny, *Computer Physics Communications* **174**, 273 (2006).